Parameter Selection by GCV and a χ^2 test within Iterative Methods for ℓ_1-regularized Inverse Problems

Brian Sweeney*, Rosemary Renaut*, and Malena I. Español*

Abstract. ℓ_1 regularization is used to preserve edges or enforce sparsity in a solution to an inverse problem. We investigate the Split Bregman and the Majorization-Minimization iterative methods that turn this non-smooth minimization problem into a sequence of steps that include solving an ℓ_2-regularized minimization problem. We consider selecting the regularization parameter in the inner generalized Tikhonov regularization problems that occur at each iteration in these ℓ_1 iterative methods. The generalized cross validation and χ^2 degrees of freedom methods are extended to these inner problems. In particular, for the χ^2 method this includes extending the χ^2 result for problems in which the regularization operator has more rows than columns, and showing how to use the A−weighted generalized inverse to estimate prior information at each inner iteration. Numerical experiments for image deblurring problems demonstrate that it is more effective to select the regularization parameter automatically within the iterative schemes than to keep it fixed for all iterations. Moreover, an appropriate regularization parameter can be estimated in the early iterations and used fixed to convergence.

1. Introduction. We are interested in solving discrete ill-posed inverse problems where we have an observation $\tilde{\mathbf{b}}$ from an unknown input $\mathbf{x}$, connected by the linear system $\tilde{\mathbf{A}}\mathbf{x} \approx \tilde{\mathbf{b}}$, where $\tilde{\mathbf{A}} \in \mathbb{R}^{m \times n}$, $\tilde{\mathbf{b}} \in \mathbb{R}^m$, and $\mathbf{x} \in \mathbb{R}^n$. We assume that $\tilde{\mathbf{A}}$ is ill-conditioned and that $\tilde{\mathbf{b}}$ is contaminated by additive Gaussian noise: $\tilde{\mathbf{b}} = \tilde{\mathbf{b}}_{true} + \boldsymbol{\epsilon}_{\tilde{\mathbf{b}}}$, where $\boldsymbol{\epsilon}_{\tilde{\mathbf{b}}} \sim \mathcal{N}(\mathbf{0}, \mathbf{C_b})$ is a Gaussian noise vector. The matrix $\mathbf{C_b}$ is a symmetric positive definite (SPD) covariance matrix. Since $\tilde{\mathbf{A}}$ is ill-conditioned, solving the problem with direct inversion will lead to a noisy solution. Therefore, we impose regularization to make the problem well-posed. One option is to apply Tikhonov regularization [37] and solve the minimization problem

$$(1.1) \qquad \min_{\mathbf{x}} \left\{ \frac{1}{2} \|\tilde{\mathbf{A}}\mathbf{x} - \tilde{\mathbf{b}}\|^2_{\mathbf{W_b}} + \frac{\lambda^2}{2} \|\mathbf{L}\mathbf{x}\|^2_2 \right\},$$

where $\mathbf{W_b} = \mathbf{C_b^{-1}}$ and the weighted norm is defined as $\|\mathbf{z}\|^2_{\mathbf{W_b}} = \mathbf{z}^\top \mathbf{W_b} \mathbf{z}$ for any vector $\mathbf{z}$. Here, λ is a regularization parameter that balances the data fidelity term and the regularization term. The regularization matrix $\mathbf{L} \in \mathbb{R}^{p \times n}$ is often selected as the discretization of a derivative operator [21], and the regularization term then minimizes the corresponding derivative of $\mathbf{x}$. Other matrices, such as discrete wavelet [15] or framelet transforms [9, 39], can be used to minimize the value of $\mathbf{x}$ in the corresponding subspaces.

We can whiten the noise in the data by multiplying out the weighted norm in (1.1), giving

---

*School of Mathematical and Statistical Sciences, Arizona State University, Tempe, AZ (bfsweene@asu.edu, renaut@asu.edu, and malena.espanol@asu.edu)

the minimization problem

$$(1.2) \qquad \min_{\mathbf{x}} \left\{ \frac{1}{2} \left\| \mathbf{A}\mathbf{x} - \mathbf{b} \right\|_2^2 + \frac{\lambda^2}{2} \left\| \mathbf{L}\mathbf{x} \right\|_2^2 \right\},$$

where

$$(1.3) \qquad \mathbf{A} = \mathbf{W_b}^{1/2} \tilde{\mathbf{A}} \text{ and } \mathbf{b} = \mathbf{W_b}^{1/2} \tilde{\mathbf{b}}.$$

Now, $\mathbf{b} = \mathbf{b}_{true} + \boldsymbol{\epsilon_b}$, where $\boldsymbol{\epsilon_b} \sim \mathcal{N}(\mathbf{0}, \mathbf{I}_m)$. For the rest of the paper, we use the weighted $\mathbf{A}$ and $\mathbf{b}$, meaning that we assume $\boldsymbol{\epsilon_b} \sim \mathcal{N}(\mathbf{0}, \mathbf{I}_m)$.

One benefit of the ℓ_2 regularization problem (1.2) is that it has a closed-form solution, but it also makes solutions smooth. If the true solution has edges or is sparse, smooth solutions may not be desirable. For these types of solutions, the 1-norm is typically used as it preserves edges and enforces sparsity. This gives the ℓ_1-regularized problem

$$(1.4) \qquad \min_{\mathbf{x}} \left\{ \frac{1}{2} \left\| \mathbf{A}\mathbf{x} - \mathbf{b} \right\|_2^2 + \mu \left\| \mathbf{L}\mathbf{x} \right\|_1 \right\}.$$

Here, μ is a regularization parameter and $\mathbf{L}$ is a regularization matrix as in (1.2). One special case of ℓ_1 regularization is total variation (TV) regularization, first introduced in [35], where $\mathbf{L}$ is the discretization of the first derivative. Unlike (1.2), (1.4) does not have a closed-form solution. Matrices $\mathbf{A}$ and $\mathbf{L}$ may not have full rank, but we assume the invertibility condition

$$(1.5) \qquad \mathcal{N}(\mathbf{A}) \cap \mathcal{N}(\mathbf{L}) = \emptyset.$$

In both (1.2) and (1.4), the value of the regularization parameter has a large impact on the solution. For (1.2), there are many methods for selecting λ, including the discrepancy principle (DP) [20, 32], the unbiased predictive risk estimator (UPRE) [28], generalized cross validation (GCV) [17], the L-curve criterion [19], and the χ^2 degrees of freedom (dof) test [31]. If training data sets are available, there are also learning approaches that can be used to select λ [8, 11]. Many of these methods make use of the closed-form solution, which makes applying them to (1.4) difficult. As a result, there are fewer parameter selection methods for (1.4). Some methods have been extended to selecting μ in (1.4), including DP [3, 27] and the L-curve [23, 40]. With the L-curve, the two terms in (1.4) are plotted against each other on a log-scale, and μ is selected at the corner of the corresponding curve. There are also methods in the statistics community for selecting μ based upon the degrees of freedom in the solution [36], including the χ^2 dof test for the TV problem [29]. Here we focus on extending the GCV and χ^2 methods within the iterative algorithms for the solution of the TV problem.

Main contributions: We consider the Split Bregman (SB) and Majorization-Minimization (MM) iterative methods for solving the ℓ_1 regularization problem. Both iterative methods solve an ℓ_2-ℓ_2 minimization problem of the form

$$(1.6) \qquad \min_{\mathbf{x}} J(\mathbf{x}) = \min_{\mathbf{x}} \left\{ \frac{1}{2} \left\| \mathbf{A}\mathbf{x} - \mathbf{b} \right\|_2^2 + \frac{\lambda^2}{2} \left\| \mathbf{L}\mathbf{x} - \mathbf{h}^{(k)} \right\|_2^2 \right\},$$

at the kth iteration. Based on this minimization problem, we consider methods for selecting λ every iteration. In particular, we extend GCV and the χ^2 dof test to this inner problem.

To apply the χ^2 dof test, we use the **A**-weighted generalized inverse of **L** to replace $\mathbf{h}^{(k)}$ in (1.6) so that we can apply the χ^2 test with the regularization term $\|\mathbf{L}(\mathbf{x} - \mathbf{x}_0)\|_2$ for a suitably defined reference vector $\mathbf{x}_0$. We also extend the non-central χ^2 test for this configuration, and provide a new result on the degrees of freedom for problems in which **L** has more rows than columns, as needed for 2D cases. Through numerical examples, we show that these selection methods can be applied at each iteration to achieve results that are comparable to finding a fixed λ that is optimal with respect to the minimization of the relative error in the solution. We also demonstrate that GCV and the χ^2 dof test can be used in the initial iterations to find a suitable regularization parameter. The methods zoom in on a parameter that is then held fixed when the change in the parameter per iteration is less than a given tolerance. This works well and is less expensive than estimating λ by GCV or the χ^2 estimator at every iteration.

The organization of this paper is as follows. In section 2, we review SB and MM iterative methods. In section 3, we develop three methods to find the iterative dependent regularization parameter for the Tikhonov problem that arises in both the SB and MM algorithm, focusing on the GCV in subsection 3.1, the χ^2 dof test in subsection 3.2, and the non-central χ^2 dof test in subsection 3.2.1. These methods are validated on numerical examples in section 4. Conclusions are presented in section 5.

2. Iterative methods for ℓ_1 regularization. In this section, we review the split Bregman (SB) and the Majorization-Minimization (MM) methods, which share the inner problem of the form (1.6). Both methods are applied to the weighted **A** and **b** as defined in (1.3).

2.1. The Split Bregman method. In the SB method, introduced by Goldstein and Osher [16], the problem (1.4) is rewritten as a constrained optimization problem

$$(2.1) \qquad \min_{\mathbf{x}} \left\{ \frac{1}{2} \|\mathbf{Ax} - \mathbf{b}\|_2^2 + \mu\|\mathbf{d}\|_1 \right\} \quad \text{s.t. } \mathbf{Lx} = \mathbf{d}.$$

Problem (2.1) can then be converted to an unconstrained optimization problem

$$(2.2) \qquad \min_{\mathbf{x},\mathbf{d}} \left\{ \frac{1}{2} \|\mathbf{Ax} - \mathbf{b}\|_2^2 + \frac{\lambda^2}{2} \|\mathbf{Lx} - \mathbf{d}\|_2^2 + \mu\|\mathbf{d}\|_1 \right\},$$

which can be solved by a series of minimizations and updates known as the SB iteration

$$(2.3) \qquad (\mathbf{x}^{(k+1)}, \mathbf{d}^{(k+1)}) = \arg\min_{\mathbf{x},\mathbf{d}} \left\{ \frac{1}{2} \|\mathbf{Ax} - \mathbf{b}\|_2^2 + \frac{\lambda^2}{2} \|\mathbf{Lx} - \mathbf{d}^{(k)} + \mathbf{g}^{(k)}\|_2^2 + \mu\|\mathbf{d}\|_1 \right\}$$

$$(2.4) \qquad \mathbf{g}^{(k+1)} = \mathbf{g}^{(k)} + (\mathbf{Lx}^{(k+1)} - \mathbf{d}^{(k+1)}).$$

In Problem (2.3) the vectors **x** and **d** can be found separately as

$$(2.5) \qquad \mathbf{x}^{(k+1)} = \arg\min_{\mathbf{x}} \left\{ \frac{1}{2} \|\mathbf{Ax} - \mathbf{b}\|_2^2 + \frac{\lambda^2}{2} \|\mathbf{Lx} - (\mathbf{d}^{(k)} - \mathbf{g}^{(k)})\|_2^2 \right\}$$

$$(2.6) \qquad \mathbf{d}^{(k+1)} = \arg\min_{\mathbf{d}} \left\{ \mu\|\mathbf{d}\|_1 + \frac{\lambda^2}{2} \|\mathbf{d} - (\mathbf{Lx}^{(k+1)} + \mathbf{g}^{(k)})\|_2^2 \right\}.$$

Here, and in the update (2.4), **g** is the vector of Lagrange multipliers.

Clearly, the solution of (2.3) depends on parameters λ and μ that are often chosen as problem-dependent known values. In this investigation, we hold the ratio $\tau = \mu^{(k)}/(\lambda^{(k)})^2$ fixed and explore methods to select $\lambda^{(k)}$ at each iteration. With these parameters, $\mu^{(k)} = \tau(\lambda^{(k)})^2$ and (2.6) becomes

$$(2.7) \qquad \mathbf{d}^{(k+1)} = \arg\min_{\mathbf{d}} \left\{ \tau\|\mathbf{d}\|_1 + \frac{1}{2}\|\mathbf{d} - (\mathbf{L}\mathbf{x}^{(k+1)} + \mathbf{g}^{(k)})\|_2^2 \right\}.$$

Since the elements of $\mathbf{d}$ are decoupled in (2.7), $\mathbf{d}^{(k+1)}$ can be computed using shrinkage operators. Each element is given by

$$d_j^{(k+1)} = \text{shrink}\left((\mathbf{L}\mathbf{x}^{(k+1)})_j + g_j^{(k)}, \tau \right),$$

where $\text{shrink}(x, \tau) = \text{sign}(x) \cdot \max(|x| - \tau, 0)$. Algorithm 2.1 summarizes the SB algorithm. Notice that SB is related to applying the alternating direction method of multipliers (ADMM) to the augmented Lagrangian in (2.2) [14].

Algorithm 2.1 The SB Method for the ℓ_2-ℓ_1 Problem (1.4)

Input: $\mathbf{A}, \mathbf{b}, \mathbf{L}, \tau, \mathbf{d}^{(0)} = \mathbf{g}^{(0)} = \mathbf{0}$
Output: x

1: **for** $k = 0, 1, \ldots$ until convergence **do**
2:      Estimate $\lambda^{(k)}$
3:      $\mathbf{x}^{(k+1)} = \arg\min_{\mathbf{x}} \left\{ \frac{1}{2}\|\mathbf{A}\mathbf{x} - \mathbf{b}\|_2^2 + \frac{(\lambda^{(k)})^2}{2}\|\mathbf{L}\mathbf{x} - (\mathbf{d}^{(k)} - \mathbf{g}^{(k)})\|_2^2 \right\}$
4:      $\mathbf{d}^{(k+1)} = \arg\min_{\mathbf{d}} \left\{ \tau\|\mathbf{d}\|_1 + \frac{1}{2}\|\mathbf{d} - (\mathbf{L}\mathbf{x}^{(k+1)} + \mathbf{g}^{(k)})\|_2^2 \right\}$
5:      $\mathbf{g}^{(k+1)} = \mathbf{g}^{(k)} + \left(\mathbf{L}\mathbf{x}^{(k+1)} - \mathbf{d}^{(k+1)} \right)$
6: **end for**

2.2. The Majorization-Minimization method. Another iterative method for solving (1.4) is the MM method. MM is an optimization method that utilizes two steps: majorization and minimization [26]. In the majorization step, the function is majorized with a surrogate convex function. The convexity of this function is then utilized in the minimization step. MM is applied to (1.4) in [25], where it is combined with the generalized Krylov subspace (GKS) method to solve large-scale image restoration problems. In MM-GKS, the Krylov subspace is enlarged at each iteration, and MM is then applied to the problem in the subspace. Instead of building a Krylov subspace as in [7, 25, 33], we will apply the MM method directly to (1.4), using the fixed quadratic majorant from [25]. Other ways for majorizing (1.4) include fixed and adaptive quadratic majorants [1, 7, 33].

With this majorant, the minimization problem at each kth iteration is

$$(2.8) \qquad \min_{\mathbf{x}} \left\{ \frac{1}{2}\|\mathbf{A}\mathbf{x} - \mathbf{b}\|_2^2 + \frac{\lambda^2}{2}\|\mathbf{L}\mathbf{x} - \mathbf{w}_{reg}^{(k)}\|_2^2 \right\},$$

where $\lambda = (\mu/\varepsilon)^{1/2}$ and

$$(2.9) \qquad \mathbf{w}_{reg}^{(k)} = \mathbf{u}^{(k)} \left(1 - \left(\frac{\varepsilon^2}{(\mathbf{u}^{(k)})^2 + \varepsilon^2} \right)^{\frac{1}{2}} \right)$$

with $\mathbf{u}^{(k)} = \mathbf{L}\mathbf{x}^{(k)}$. All operations in (2.9) are component-wise. Again, the parameters can be selected at each iteration. Here, as with our approach for the SB algorithm, we select $\lambda^{(k)}$ at each iteration and fix ε as in [5] for MM-GKS. Algorithm 2.2 summarizes the MM algorithm.

Algorithm 2.2 The MM Method for the ℓ_2-ℓ_1 Problem (1.4) with a Fixed Quadratic Majorant

---

Input: $\mathbf{A}, \mathbf{b}, \mathbf{L}, \mathbf{x}^{(0)}, \varepsilon$
Output: $\mathbf{x}$
1: **for** $k = 0, 1, \ldots$ until convergence **do**
2: $\quad$ $\mathbf{u}^{(k)} = \mathbf{L}\mathbf{x}^{(k)}$
3: $\quad$ $\mathbf{w}_{reg}^{(k)} = \mathbf{u}^{(k)} \left(1 - \left(\frac{\varepsilon^2}{\left(\mathbf{u}^{(k)}\right)^2 + \varepsilon^2} \right)^{\frac{1}{2}} \right)$
4: $\quad$ Estimate $\lambda^{(k)}$
5: $\quad$ $\mathbf{x}^{(k+1)} = \arg\min_{\mathbf{x}} \left\{ \frac{1}{2}\|\mathbf{A}\mathbf{x} - \mathbf{b}\|_2^2 + \frac{\left(\lambda^{(k)}\right)^2}{2}\|\mathbf{L}\mathbf{x} - \mathbf{w}_{reg}^{(k)}\|_2^2 \right\}$
6: **end for**

2.3. The inner minimization problem. At each iteration k in both SB and MM we solve a problem of the form as given by (1.6) with the regularization parameter λ replaced by $\lambda^{(k)}$ (see (2.5) for SB and (2.8) for MM). In SB, $\mathbf{h}^{(k)} = \mathbf{d}^{(k)} - \mathbf{g}^{(k)}$, while in MM, $\mathbf{h}^{(k)} = \mathbf{w}_{reg}^{(k)}$. We focus on (1.6) and regularization parameter estimation methods for finding $\lambda^{(k)}$ that can be used within each iteration of SB and MM.

2.4. Matrix decompositions. To analyze (1.6), we will use the generalized singular value decomposition (GSVD) [18, 20, 24], which is a joint matrix decomposition of two matrices $\mathbf{A}$ and $\mathbf{L}$. Consider $\mathbf{A} \in \mathbb{R}^{m \times n}$ and $\mathbf{L} \in \mathbb{R}^{p \times n}$, and let $\tilde{n} = \text{rank}(\mathbf{L})$. When $m \geq n$ and the invertibility condition (1.5) is satisfied, there exist orthogonal matrices $\mathbf{U} \in \mathbb{R}^{m \times m}$ and $\mathbf{V} \in \mathbb{R}^{p \times p}$ and an invertible matrix $\mathbf{X} \in \mathbb{R}^{n \times n}$ such that

$$(2.10) \qquad \mathbf{A} = \mathbf{U}\tilde{\mathbf{\Upsilon}}\mathbf{X}^{-1}, \quad \mathbf{L} = \mathbf{V}\tilde{\mathbf{M}}\mathbf{X}^{-1},$$

where

$$\tilde{\mathbf{\Upsilon}} = \begin{bmatrix} \mathbf{\Upsilon} & \mathbf{0}_{\tilde{n} \times (n-\tilde{n})} \\ \mathbf{0}_{(n-\tilde{n}) \times \tilde{n}} & \mathbf{I}_{(n-\tilde{n}) \times (n-\tilde{n})} \\ \mathbf{0}_{(m-n) \times \tilde{n}} & \mathbf{0}_{(m-n) \times (n-\tilde{n})} \end{bmatrix}, \qquad \mathbf{\Upsilon} = \text{diag}(\upsilon_1, \ldots, \upsilon_{\tilde{n}}),$$

$$\tilde{\mathbf{M}} = \begin{bmatrix} \mathbf{M} & \mathbf{0}_{\tilde{n} \times (n-\tilde{n})} \\ \mathbf{0}_{(p-\tilde{n}) \times \tilde{n}} & \mathbf{0}_{(p-\tilde{n}) \times (n-\tilde{n})} \end{bmatrix}, \qquad \mathbf{M} = \text{diag}(\mu_1, \ldots, \mu_{\tilde{n}}),$$

with $0 \leq \upsilon_1 \leq \cdots \leq \upsilon_{\tilde{n}} < 1$, $1 \geq \mu_1 \geq \cdots \geq \mu_{\tilde{n}} > 0$, and $\upsilon_i^2 + \mu_i^2 = 1$ for $i = 1, \ldots, \tilde{n}$. For $i = 1, \ldots, \tilde{n}$, $\gamma_i = \upsilon_i/\mu_i$ are called the generalized singular values. Here, and throughout, we use $\mathbf{I}_{a \times b}$ and $\mathbf{0}_{a \times b}$ to denote the identity and zero matrices, respectively, of dimension $a \times b$ and which may possibly have no rows or no columns.

The GSVD is helpful for analyzing the properties of the solutions as a function of λ and, consequently, for analyzing regularization methods. On the other hand, computationally, it is only helpful for small problems. Other joint decompositions, such as the discrete Fourier

transform or the discrete cosine transform, can be practical for larger problems, as we will see in the numerical results section.

3. Estimation of the regularization parameter. In this section, we present two methods for finding the regularization parameter in the iterative updates for the SB and MM methods. We consider in subsection 3.1 the GCV method and in subsection 3.2 the χ^2 dof test. Note that while the χ^2 dof test requires that $\mathbf{C_b}$ is known, there is no such requirement for the GCV method. We also consider in subsection 3.2.1 a non-central χ^2 formulation adapted to the iteration in the SB algorithm.

3.1. The method of generalized cross validation. GCV [2, 17] is a parameter selection method that selects λ to minimize predictive risk. GCV has been applied to the generalized Tikhonov problem (1.2), which has the solution $\mathbf{x}_\lambda = \mathbf{A}_\lambda^\sharp \mathbf{b}$, where $\mathbf{A}_\lambda^\sharp$ is the influence matrix defined by $\mathbf{A}_\lambda^\sharp = \mathbf{A_L}^{-1} \mathbf{A}^\top$ with $\mathbf{A_L} = \mathbf{A}^\top \mathbf{A} + \lambda^2 \mathbf{L}^\top \mathbf{L}$. In GCV, λ is selected to minimize the GCV function

$$G(\lambda) = \frac{\|\mathbf{A}\mathbf{x}_\lambda - \mathbf{b}\|_2^2}{\left[\mathrm{Tr}\,(\mathbf{I} - \mathbf{A}_\lambda)\right]^2}, \tag{3.1}$$

where $\mathbf{A}_\lambda = \mathbf{A}\mathbf{A}_\lambda^\sharp$ is the resolution matrix. GCV has also been extended to other regularization problems [10]. Formulae for the GCV to solve (1.2) in terms of the GSVD of $\{\mathbf{A}, \mathbf{L}\}$ are given in [12, 31, 38] for different orderings of the sizes for m, n, p.

In Appendix A, we discuss how GCV is applied to (1.6) which, replacing $\mathbf{h}^{(k)}$ by $\mathbf{h}$, has the solution

$$\mathbf{x}_\lambda = \mathbf{A_L}^{-1}(\mathbf{A}^\top \mathbf{b} + \lambda^2 \mathbf{L}^\top \mathbf{h}) = \mathbf{A}_\lambda^\sharp \mathbf{b} + \mathbf{L}_\lambda^\sharp \mathbf{h}, \tag{3.2}$$

where $\mathbf{L}_\lambda^\sharp = \lambda^2 \mathbf{A_L}^{-1} \mathbf{L}^\top$. The GCV function $G(\lambda)$ for (1.6) is again given by (3.1) but now with $\mathbf{x}_\lambda$ given by (3.2). For completeness, the GCV function for $n \geq p$ and $p > n$, is given by

$$G(\lambda) = \frac{\left\|\sum_{i=1}^{\tilde{n}} \frac{\lambda^2 \gamma_i (\mathbf{v}_i^\top \mathbf{h})}{\gamma_i^2 + \lambda^2} - \sum_{i=1}^{\tilde{n}} \frac{\lambda^2 (\mathbf{u}_i^\top \mathbf{b})}{\gamma_i^2 + \lambda^2} - \sum_{i=n+1}^{m} \mathbf{u}_i^\top \mathbf{b}\right\|_2^2}{\left[\max(m - n, 0) + \sum_{i=1}^{\tilde{n}} \frac{\lambda^2}{\gamma_i^2 + \lambda^2}\right]^2}. \tag{3.3}$$

Notice that we ignore any sum in which the lower limit is greater than the upper limit.

3.2. The χ^2 degrees of freedom test. At each iteration in SB and MM, we minimize the functional $J(\mathbf{x})$ in (1.6). The χ^2 dof test is a parameter selection method that treats $\mathbf{x}$ as a random variable and utilizes the distribution of the functional evaluated at its minimizer to select λ [30]. In [31], the χ^2 dof test is applied to the functional $J_L(\mathbf{x})$ which is defined by

$$J_L(\mathbf{x}) = \|\mathbf{A}\mathbf{x} - \mathbf{b}\|_2^2 + \|\mathbf{L}(\mathbf{x} - \mathbf{x}_0)\|_{\mathbf{W_h}}^2. \tag{3.4}$$

Here, $\mathbf{x}_0$ is a reference vector of prior information on $\mathbf{x}$. We assume that $\mathbf{x}_0 = \bar{\mathbf{x}}$, where $\bar{\mathbf{x}}$ is the expected value of $\mathbf{x}$. It is also assumed in [31] that $\mathbf{L}$ has fewer rows than columns, $p \leq n$, and $\mathbf{L}(\mathbf{x} - \mathbf{x}_0) = \boldsymbol{\epsilon_h}$, where $\boldsymbol{\epsilon_h} \sim \mathcal{N}(\mathbf{0}, \mathbf{C_h})$ and $\mathbf{C_h}$ is a SPD covariance matrix.

The matrix $\mathbf{W_h} = \mathbf{C_h^{-1}}$ is then the corresponding precision matrix. We also suppose that the model errors $\mathbf{x} - \mathbf{x}_0 = \boldsymbol{\epsilon}_\mathbf{L}$ are normally distributed with covariance $\mathbf{C_L}$. From this, $\mathbf{b} \sim \mathcal{N}(\mathbf{A}\overline{\mathbf{x}}, \mathbf{I}_m + \mathbf{A}\mathbf{C_L}\mathbf{A}^\top)$. Then, in [31, Theorem 3.1], it is shown that for large m and for given $\mathbf{W_h}$, J_L is a random variable that follows a χ^2 distribution with $m + p - n$ degrees of freedom.

The goal of the χ^2 method is then to find $\mathbf{W_h}$ so that $J_L(\mathbf{x})$ most resembles a χ^2 distribution with the appropriate degrees of freedom. In [34], the χ^2 dof test for (3.4) is extended to the case when $\mathbf{x}_0 \neq \overline{\mathbf{x}}$, in which case $J_L(\mathbf{x})$ follows a non-central χ^2 distribution.

Under the assumption that $\mathbf{C_h} = \lambda^{-2}\mathbf{I}_p$, we define

$$(3.5) \qquad \mathbf{x}_\lambda = \arg\min_{\mathbf{x}} J_L(\mathbf{x}) = \arg\min_{\mathbf{x}} \left\{ \|\mathbf{A}\mathbf{x} - \mathbf{b}\|_2^2 + \lambda^2 \|\mathbf{L}(\mathbf{x} - \mathbf{x}_0)\|_2^2 \right\}.$$

$J_L(\mathbf{x})$ then follows a χ^2 distribution. In particular, the following theorem gives its degrees of freedom, that holds for $p > n$ and $p \leq n$.

Theorem 3.1. *Suppose that* $\mathbf{A}\mathbf{x} - \mathbf{b} \sim \mathcal{N}(\mathbf{0}, \mathbf{I}_m)$, $\mathbf{L}(\mathbf{x} - \mathbf{x}_0) \sim \mathcal{N}(\mathbf{0}, \lambda^{-2}\mathbf{I}_p)$, $m \geq n$, *and* $\tilde{n} = rank(\mathbf{L})$. *For a given* λ *and the corresponding solution* $\mathbf{x}_\lambda$, $J_L(\mathbf{x}_\lambda)$ *is a random variable that follows a* χ^2 *distribution with* $\tilde{n} + \max(m - n, 0)$ *degrees of freedom.*

Proof. The case when $m \geq n \geq p$ is given in [31, Theorem 3.1]. For the general case when $m \geq n$ without a restriction on p, the approach follows that given in the proof of [31, Theorem 3.1]. Noting that the solution of (3.5) is given by $\mathbf{x}_\lambda = \mathbf{x}_0 + \mathbf{A_L^{-1}}\mathbf{A}^\top\mathbf{r}$, and using the GSVD of $\{\mathbf{A}, \mathbf{L}\}$ in (2.10), $J_L(\mathbf{x}_\lambda)$ is given by

$$J_L(\mathbf{x}_\lambda) = \|\mathbf{A}\mathbf{x}_0 + \mathbf{A}\mathbf{A_L^{-1}}\mathbf{A}^\top\mathbf{r} - \mathbf{b}\|_2^2 + \lambda^2\|\mathbf{L}\mathbf{A_L^{-1}}\mathbf{A}^\top\mathbf{r}\|_2^2$$

$$= \left\|\mathbf{A}\mathbf{A_L^{-1}}\mathbf{A}^\top\mathbf{r} - \mathbf{r}\right\|_2^2 + \lambda^2\|\mathbf{L}\mathbf{A_L^{-1}}\mathbf{A}^\top\mathbf{r}\|_2^2$$

$$= \|\mathbf{U}\tilde{\boldsymbol{\Upsilon}}\boldsymbol{\Phi}^{-1}\tilde{\boldsymbol{\Upsilon}}^\top\mathbf{U}^\top\mathbf{r} - \mathbf{r}\|_2^2 + \lambda^2\|\mathbf{V}\tilde{\mathbf{M}}\boldsymbol{\Phi}^{-1}\tilde{\boldsymbol{\Upsilon}}^\top\mathbf{U}^\top\mathbf{r}\|_2^2$$

$$(3.6) \qquad = \|(\tilde{\boldsymbol{\Upsilon}}\boldsymbol{\Phi}^{-1}\tilde{\boldsymbol{\Upsilon}}^\top - \mathbf{I}_m)\mathbf{s}\|_2^2 + \lambda^2\|\tilde{\mathbf{M}}\boldsymbol{\Phi}^{-1}\tilde{\boldsymbol{\Upsilon}}^\top\mathbf{s}\|_2^2,$$

where $\mathbf{s} = [s_1, \ldots, s_m]^\top = \mathbf{U}^\top\mathbf{r}$ and $\boldsymbol{\Phi} = (\tilde{\boldsymbol{\Upsilon}}^\top\tilde{\boldsymbol{\Upsilon}} + \lambda^2\tilde{\mathbf{M}}^\top\tilde{\mathbf{M}})$. We have that

$$\tilde{\boldsymbol{\Upsilon}}\boldsymbol{\Phi}^{-1}\tilde{\boldsymbol{\Upsilon}}^\top - \mathbf{I}_m = \begin{bmatrix} -\boldsymbol{\Psi} & \mathbf{0} & \mathbf{0} \\ \mathbf{0} & \mathbf{0}_{n-\tilde{n}} & \mathbf{0} \\ \mathbf{0} & \mathbf{0} & -\mathbf{I}_{m-n} \end{bmatrix} \text{ and } \tilde{\mathbf{M}}\boldsymbol{\Phi}^{-1}\tilde{\boldsymbol{\Upsilon}}^\top = \begin{bmatrix} \boldsymbol{\zeta} & \mathbf{0} \\ \mathbf{0} & \mathbf{0}_{(p-\tilde{n})\times(m-\tilde{n})} \end{bmatrix},$$

where $\boldsymbol{\Psi}, \boldsymbol{\zeta} \in \mathbb{R}^{\tilde{n}\times\tilde{n}}$ are given by

$$(3.7) \qquad \boldsymbol{\Psi} = \text{diag}\left(\frac{\lambda^2}{\gamma_1^2 + \lambda^2}, \ldots, \frac{\lambda^2}{\gamma_{\tilde{n}}^2 + \lambda^2}\right) \text{ and } \boldsymbol{\zeta} = \text{diag}\left(\frac{\gamma_1}{\gamma_1^2 + \lambda^2}, \ldots, \frac{\gamma_{\tilde{n}}}{\gamma_{\tilde{n}}^2 + \lambda^2}\right).$$

Thus, (3.6) becomes

$$J_L(\mathbf{x}_\lambda) = \sum_{i=1}^{\tilde{n}} \frac{\lambda^4}{(\gamma_i^2 + \lambda^2)^2}s_i^2 + \sum_{i=n+1}^{m} s_i^2 + \sum_{i=1}^{\tilde{n}} \frac{\lambda^2\gamma_i^2}{(\gamma_i^2 + \lambda^2)^2}s_i^2$$

$$(3.8) \qquad = \sum_{i=1}^{\tilde{n}} \frac{\lambda^2}{\gamma_i^2 + \lambda^2}s_i^2 + \sum_{i=n+1}^{m} s_i^2 = \sum_{i=1}^{\tilde{n}} k_i^2 + \sum_{i=n+1}^{m} k_i^2,$$

with $\mathbf{k} = [k_1, \ldots, k_m]^\top = \mathbf{T}\mathbf{s}$, where

$$\mathbf{T} = \begin{bmatrix} \mathbf{\Psi}^{1/2} & \mathbf{0} & \mathbf{0} \\ \mathbf{0} & \mathbf{I}_{n-\tilde{n}} & \mathbf{0} \\ \mathbf{0} & \mathbf{0} & \mathbf{I}_{m-n} \end{bmatrix}.$$

Next, we need to show that the k_i are distributed standard normal. Using the GSVD, we have that $\mathbf{V}\tilde{\mathbf{M}}\mathbf{X}^{-1}(\mathbf{x} - \mathbf{x}_0) \sim \mathcal{N}(\mathbf{0}, \lambda^{-2}\mathbf{I}_p)$. Using the properties for normally distributed vectors, we obtain $\mathbf{x} - \mathbf{x}_0 \sim \mathcal{N}(\mathbf{0}, \lambda^{-2}\mathbf{X}\operatorname{diag}(\mathbf{M}^{-2}, \mathbf{0}_{n-\tilde{n}})\mathbf{X}^{-1})$. The residual $\mathbf{r}$ then has mean zero and covariance matrix

$$\mathbf{I}_m + \lambda^{-2}\mathbf{U}\boldsymbol{\Upsilon}\begin{bmatrix} \mathbf{M}^{-2} & \mathbf{0} \\ \mathbf{0} & \mathbf{0}_{n-\tilde{n}} \end{bmatrix}\boldsymbol{\Upsilon}^\top\mathbf{U}^\top = \mathbf{U}\begin{bmatrix} \mathbf{\Psi}^{-1} & \mathbf{0} & \mathbf{0} \\ \mathbf{0} & \mathbf{I}_{n-\tilde{n}} & \mathbf{0} \\ \mathbf{0} & \mathbf{0} & \mathbf{I}_{m-n} \end{bmatrix}\mathbf{U}^\top = \mathbf{U}\mathbf{T}^{-2}\mathbf{U}^\top.$$

Thus, $\mathbf{k}$ has covariance $\mathbf{T}\mathbf{U}^\top(\mathbf{U}\mathbf{T}^{-2}\mathbf{U}^\top)\mathbf{U}\mathbf{T}^\top = \mathbf{I}_m$ and the k_i follow a standard normal distribution. Hence, $J_L(\mathbf{x}_\lambda)$ is the sum of $\tilde{n} + \max(m - n, 0)$ squared standard normal random variables. ■

When $\tilde{m}$ is large, the $\chi_{\tilde{m}}^2$ distribution can be approximated by a normal distribution with mean $\tilde{m}$ and variance $2\tilde{m}$, denoted by $\mathcal{N}(\tilde{m}, 2\tilde{m})$. We can use this approximation to find λ such that $J_L(\mathbf{x}_\lambda)$ is then approximately distributed as $\mathcal{N}(\tilde{m}, 2\tilde{m})$. As in [31], we form a $(1-\alpha)$ confidence interval to find λ:

$$\tilde{m} - z_{0.5+\alpha/2}\sqrt{2\tilde{m}} \leq J_L(\mathbf{x}_\lambda) \leq \tilde{m} + z_{0.5+\alpha/2}\sqrt{2\tilde{m}}.$$

Here, $z_{0.5+\alpha/2}$ is the relevant z-value for the standard normal distribution, which defines the bounds for the $(1 - \alpha)$ confidence interval. Defining $F(\lambda) = J_L(\mathbf{x}_\lambda) - \tilde{m}$, we apply Newton's method to λ such that

$$(3.9) \qquad -z_{0.5+\alpha/2}\sqrt{2\tilde{m}} \leq F(\lambda) \leq z_{0.5+\alpha/2}\sqrt{2\tilde{m}}.$$

The derivative of $F(\lambda)$ is $F'(\lambda) = 2\lambda\|\tilde{\mathbf{s}}\|_2^2$. Here, $\tilde{\mathbf{s}} = [\tilde{s}_1, \ldots, \tilde{s}_{\tilde{n}}]^\top$, where $\tilde{s}_i = \gamma_i s_i/(\gamma_i^2 + \lambda^2)$ for $i = 1, \ldots, \tilde{n}$. We notice immediately that for $\lambda > 0$, as required, $F' > 0$, and hence it is reasonable to use a root-finding method for λ, provided that we can find an interval in which $F(\lambda)$ changes sign. This is discussed in more detail in [31]. An example of $F(\lambda)$ is given in Figure 1(b).

The tolerance for Newton's method depends on the selection of the confidence level α. A smaller value of α makes the $(1 - \alpha)$ confidence interval larger, increasing the probability that a random value of λ satisfies (3.9). On the other hand, a larger α narrows this interval, increasing the confidence that λ satisfies the χ^2 distribution.

For SB and MM, the inner minimization problem (1.6) is not of the desired form (3.4) for the central χ^2 dof test. In particular, we need $\mathbf{L}\mathbf{x}_0$ in place of $\mathbf{h}^{(k)}$ in (1.6). To find $\mathbf{x}_0$ such that $\mathbf{h}^{(k)} \approx \mathbf{L}\mathbf{x}_0$, we will use the the $\mathbf{A}$-weighted generalized inverse of $\mathbf{L}$, denoted $\mathbf{L}_\mathbf{A}^\dagger$ [13]. In terms of the GSVD of $\{\mathbf{A}, \mathbf{L}\}$, $\mathbf{L}_\mathbf{A}^\dagger = \mathbf{X}\tilde{\mathbf{M}}^\dagger\mathbf{V}^\top$, where $\tilde{\mathbf{M}}^\dagger \in \mathbb{R}^{n \times p}$ has diagonal entries $1/\mu_i$. If $p \geq n$, then $\mathbf{L}_\mathbf{A}^\dagger = \mathbf{L}^\dagger$, where $\mathbf{L}^\dagger$ is the pseudoinverse of $\mathbf{L}$ [20]. For $p < n$, $\mathbf{L}_\mathbf{A}^\dagger \neq \mathbf{L}^\dagger$ in general.
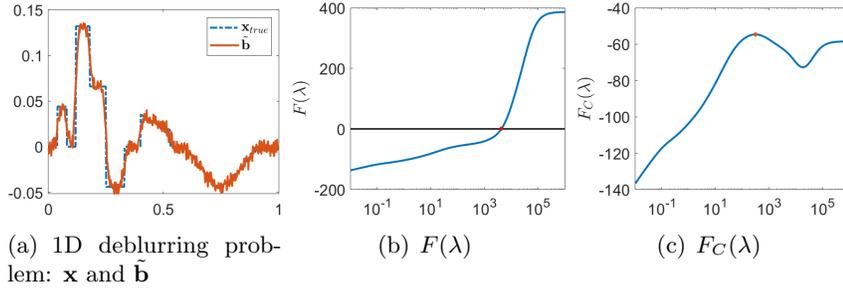
(a) 1D deblurring problem: $\mathbf{x}$ and $\tilde{\mathbf{b}}$

(b) $F(\lambda)$

(c) $F_C(\lambda)$

Figure 1. *Figure* 1(a)*:* $\mathbf{x}$ *and* $\tilde{\mathbf{b}}$ *for the 1D deblurring problem (SNR = 20). Figures* 1(b) *and* 1(c) *plot* $F(\lambda)$ *and* $F_C(\lambda)$ *for MM applied to this problem, where the selected* λ *is marked. In Figure* 1(c)*,* $F_C(\lambda)$ *is not monotonic and does not have a root.*

In terms of the GSVD of $\{\mathbf{A}, \mathbf{L}\}$, $\mathbf{L}\mathbf{L}_{\mathbf{A}}^{\dagger} = \mathbf{V}\tilde{\mathbf{M}}\tilde{\mathbf{M}}^{\dagger}\mathbf{V}^{\top}$. When $\mathbf{L}$ is invertible, and when $p \leq n$, $\tilde{\mathbf{M}}\tilde{\mathbf{M}}^{\dagger} = \mathbf{I}_p$ so $\mathbf{L}\mathbf{L}_{\mathbf{A}}^{\dagger} = \mathbf{I}_p$. In the χ^2 dof test, we will estimate $\mathbf{x}_0$ as $\mathbf{L}_{\mathbf{A}}^{\dagger}\mathbf{h}^{(k)}$ and use $\mathbf{L}\mathbf{L}_{\mathbf{A}}^{\dagger}\mathbf{h}^{(k)}$ in place of $\mathbf{h}^{(k)}$. With this, (1.6) can be rewritten in the form of (3.4). Provided that $\mathbf{x}_0$ is approximately the expected value of $\mathbf{x}$, we may use the central χ^2 dof test at each iteration of SB and MM. In the case where $\mathbf{x}_0 \not\approx \bar{\mathbf{x}}$, the central χ^2 dof test no longer applies.

3.2.1. The non-central χ^2 dof test. When $\mathbf{x}_0 \not\approx \bar{\mathbf{x}}$, $J_L(\mathbf{x})$ follows a non-central χ^2 distribution with $\tilde{m}$ degrees of freedom and non-centrality parameter c, defined by

$$c(\lambda) = \sum_{i=1}^{\tilde{n}} \frac{\lambda^2 q_i^2}{\gamma_i^2 + \lambda^2} + \sum_{i=n+1}^{m} q_i^2,$$

where $\mathbf{q} = [q_1, \ldots, q_m]^{\top} = \mathbf{U}^{\top}\mathbf{A}(\bar{\mathbf{x}} - \mathbf{x}_0)$ [34]. As with the central χ^2 dof test, the goal of the non-central test is to find λ so that $J_L \sim \chi^2(\tilde{m}, c(\lambda))$. When $\tilde{m}$ is sufficiently large, this non-central χ^2 distribution can be approximated by a normal distribution with mean $\tilde{m}+c(\lambda)$ and variance $2\tilde{m}+4c(\lambda)$. Using this approximation, we can form a $(1-\alpha)$ confidence interval to find λ:

$$\tilde{m} + c(\lambda) - z_{0.5+\alpha/2}\sqrt{2\tilde{m} + 4c(\lambda)} \leq J_L(\mathbf{x}_{\lambda}) \leq \tilde{m} + c(\lambda) + z_{0.5+\alpha/2}\sqrt{2\tilde{m} + 4c(\lambda)}.$$

Defining $F_C(\lambda) = J_L(\mathbf{x}_{\lambda}) - (\tilde{m} + c(\lambda))$, this is equivalent to solving the problem

$$(3.10) \qquad -z_{0.5+\alpha/2}\sqrt{2\tilde{m} + 4c(\lambda)} \leq F_C(\lambda) \leq z_{0.5+\alpha/2}\sqrt{2\tilde{m} + 4c(\lambda)}.$$

In this case, the derivative of $F_C(\lambda)$ is

$$(3.11) \qquad F_C'(\lambda) = 2\lambda\left(\|\tilde{\mathbf{s}}\|_2^2 - \|\tilde{\mathbf{q}}\|_2^2\right),$$

where $\tilde{\mathbf{q}} = [\tilde{q}_1, \ldots, \tilde{q}_{\tilde{n}}]^{\top}$ with $\tilde{q}_i = \gamma_i q_i/(\gamma_i^2 + \lambda^2)$ for $i = 1, \ldots, \tilde{n}$. Notice that when $\mathbf{x}_0 = \bar{\mathbf{x}}$, $\mathbf{q} = \mathbf{0}$ and the non-central test reduces to the central test.

From (3.11), it is immediate that $F_C'(\lambda)$ is not of constant sign, so $F_C(\lambda)$ may potentially have no root or multiple roots. Figure 1(c) shows an example where $F_C(\lambda)$ is not monotone

and has no root. If $F_C(\lambda)$ has a single root, we can apply Newton's method to find λ such that (3.10) holds. Otherwise, we follow the method presented in [34] to find λ such that $F_C(\lambda)$ is close to zero.

To use the non-central χ^2 dof test in SB and MM, we still rewrite (1.6) using $\mathbf{L}\mathbf{L}_{\mathbf{A}}^{\dagger}\mathbf{h}^{(k)}$ in place of $\mathbf{h}^{(k)}$. We also need to have an estimate of the expected value of $\mathbf{x}$ to use as $\overline{\mathbf{x}}$ in the test. Within both SB and MM, one option is to use the current solution $\mathbf{x}^{(k)}$ as an approximation of $\overline{\mathbf{x}}$. Another option in SB is to estimate $\overline{\mathbf{x}}$ using $\mathbf{L}_{\mathbf{A}}^{\dagger}\mathbf{d}^{(k)}$ since $\mathbf{d}$ in SB approximates $\mathbf{L}\mathbf{x}$ quite well. We will use $\overline{\mathbf{x}} = \mathbf{x}^{(k)}$, assuming that at a given step of the iteration we are looking to reduce the noise around the current estimate, and that for increasing k with convergence we have $\overline{\mathbf{x}} = \lim_k \mathbf{x}^{(k)}$.

4. Numerical examples. In this section, we apply SB and MM to two deblurring problems to test the parameter selection methods presented in section 3. To compare methods, we will use the relative error (RE) which is defined by

$$\mathrm{RE} = \frac{\|\mathbf{x} - \mathbf{x}_{true}\|_2}{\|\mathbf{x}_{true}\|_2}.$$

The RE is a measure of how close the current solution is to the true solution $\mathbf{x}_{true}$. In practice, $\mathbf{x}_{true}$ is unknown, so to understand when these methods have converged, we will consider the relative change in $\mathbf{x}$ and λ. The relative change in $\mathbf{x}$, defined as

$$(4.1) \qquad \mathrm{RC}(\mathbf{x}^{(k)}) = \frac{\left\|\mathbf{x}^{(k)} - \mathbf{x}^{(k-1)}\right\|_2}{\left\|\mathbf{x}^{(k-1)}\right\|_2},$$

measures how much the solution is changing at a given iteration. If it is below a specified tolerance, $\mathrm{TOL}_{\mathbf{x}}$, then the solution is not changing much and we can consider the solution to be converged and stop iterating. This tolerance should depend on the noise level. Because we use the weighted data fidelity term with $\mathbf{A}$ and $\mathbf{b}$ as defined in (1.3), it is sufficient to use a fixed tolerance, here $\mathrm{TOL}_{\mathbf{x}} = 0.001$, for all noise levels.

The relative change in λ^2,

$$(4.2) \qquad \mathrm{RC}((\lambda^{(k)})^2) = \frac{|(\lambda^{(k)})^2 - (\lambda^{(k-1)})^2|}{|(\lambda^{(k-1)})^2|},$$

measures how much λ^2 changes from one iteration to the next. If $\mathrm{RC}((\lambda^{(k)})^2) < \mathrm{TOL}_{\lambda}$, then, we can stop selecting λ and fix it at the current value until convergence. This reduces the computational cost from applying the parameter selection method at every iteration. In both (4.1) and (4.2), we assume, without loss of generality, that the denominator is non-zero.

For each example, we select λ at each iteration with the different selection methods and compare the results to the *optimal* fixed λ. To find this *optimal* λ, we run each example to completion for 121 values of λ that are logarithmically spaced from 10^{-1} to 10^3 and select as *optimal* the λ that has the smallest RE at completion. For the χ^2 dof tests, we use $\mathbf{x}_0^{SB} = \mathbf{L}_{\mathbf{A}}^{\dagger}(\mathbf{d} - \mathbf{g})$ and $\mathbf{x}_0^{MM} = \mathbf{L}_{\mathbf{A}}^{\dagger}(\mathbf{w}_{reg})$. For the non-central χ^2 dof test, we use $\overline{\mathbf{x}} = \mathbf{x}^{(k)}$. Furthermore, in all the numerical experiments we use a confidence level of $\alpha = 0.999$ for the χ^2 dof test.
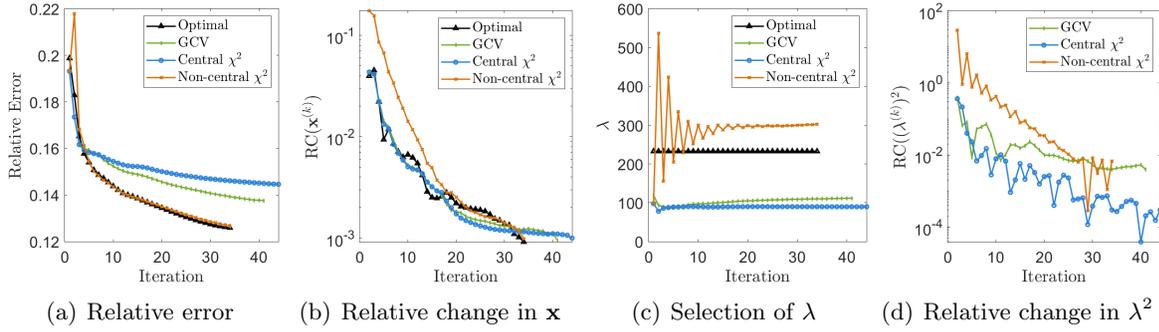
(a) Relative error   (b) Relative change in $\mathbf{x}$ (c) Selection of λ (d) Relative change in λ^2

Figure 2. *Results for SB applied to Figure 1(a) where λ is fixed at the optimal $\lambda = 232.6$, or selected at each iteration with GCV or the χ^2 dof tests. Figure 2(a) plots the RE by iteration, Figure 2(b) plots the relative change in $\mathbf{x}$, Figure 2(c) plots the λ selected, and Figure 2(d) plots the relative change in λ^2.*

4.1. A 1D example. For the first numerical example, we will consider a 1D blurring problem. The matrix $\tilde{\mathbf{A}} \in \mathbb{R}^{N \times N}$ is symmetric Toeplitz where the first row is

$$(4.3) \qquad \mathbf{z} = \frac{1}{2\pi\sigma} \left[\exp\left(\frac{-[0:\text{band}-1]^2}{2\sigma} \right) \quad \mathbf{0}_{N-\text{band}} \right].$$

We use $N = 512$, $\sigma = 24$, and band $= 60$. Gaussian noise with SNR $= 20$ is added to the blurred signal to produce $\tilde{\mathbf{b}}$. The true signal $\mathbf{x}_{true}$ and the blurred and noisy data $\tilde{\mathbf{b}}$ are given in Figure 1(a). We solve this problem with SB and MM for $\mathbf{L} \in \mathbb{R}^{(N-1) \times N}$ defined as the discretization of the first derivative operator with zero boundary conditions:

$$\mathbf{L} = \begin{bmatrix} -1 & 1 & 0 & \cdots & & 0 \\ 0 & -1 & 1 & 0 & \cdots & 0 \\ \vdots & & \ddots & \ddots & & \vdots \\ 0 & \cdots & 0 & -1 & 1 & 0 \\ 0 & \cdots & & 0 & -1 & 1 \end{bmatrix}.$$

Given the size of this 1D example, we use the GSVD of $\{\mathbf{A}, \mathbf{L}\}$ to solve the inner problem in both SB and MM. We use three different methods for selecting λ at each iteration: GCV, the central χ^2 dof test, and the non-central χ^2 dof test. These are compared with the results obtained using the *optimal* fixed λ. In the χ^2 dof tests, the confidence level of $\alpha = 0.999$ corresponds to a bound of 0.042 on $F(\lambda)$. For $F_C(\lambda)$, the bound will be at least 0.042 but it increases with λ and $\left\| \mathbf{x}^{(k)} - \mathbf{x}_0 \right\|_2$. In this example, the bound on $F_C(\lambda)$ ranges from 0.042 to 0.1, with the larger value obtained in the initial iterations. For the three selection methods, $\text{TOL}_\lambda = 0.01$ is applied and compared with selecting parameters at every iteration.

4.1.1. Split Bregman. In SB, we set $\tau = 0.005$ as $\text{RC}(\mathbf{x}^{(k)})$ decreases smoothly until convergence for this τ. The value of τ depends on the noise level, where in this case, a larger value of τ leads to $\text{RC}(\mathbf{x}^{(k)})$ spiking at different iterations, even for a fixed value of λ. The *optimal* fixed λ in this case is $\lambda = 232.6$. The results for SB with these selection methods are shown in Figure 2, with solutions provided in Figure 3. The values of λ selected by the non-central χ^2 dof test oscillate in the first 15 iterations. This is to be anticipated with the choice
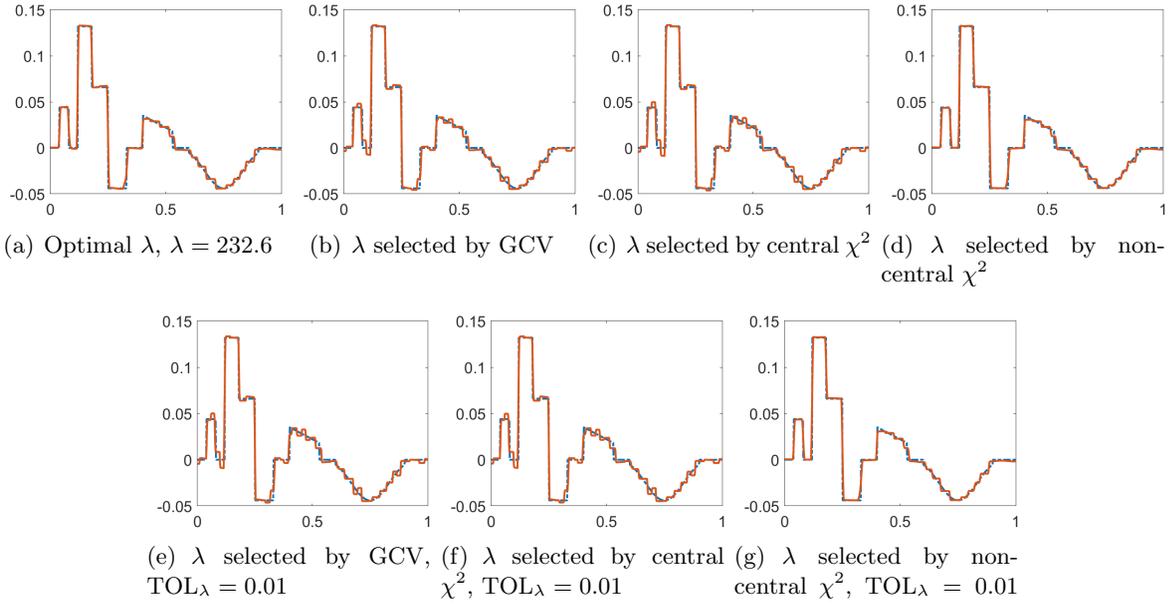
(a) Optimal λ, $\lambda = 232.6$ (b) λ selected by GCV   (c) λ selected by central χ^2 (d) λ selected by non-central χ^2

(e) λ selected by GCV, $\mathrm{TOL}_\lambda = 0.01$ (f) λ selected by central χ^2, $\mathrm{TOL}_\lambda = 0.01$ (g) λ selected by non-central χ^2, $\mathrm{TOL}_\lambda = 0.01$

Figure 3. *SB solutions at convergence for Figure 1(a).*

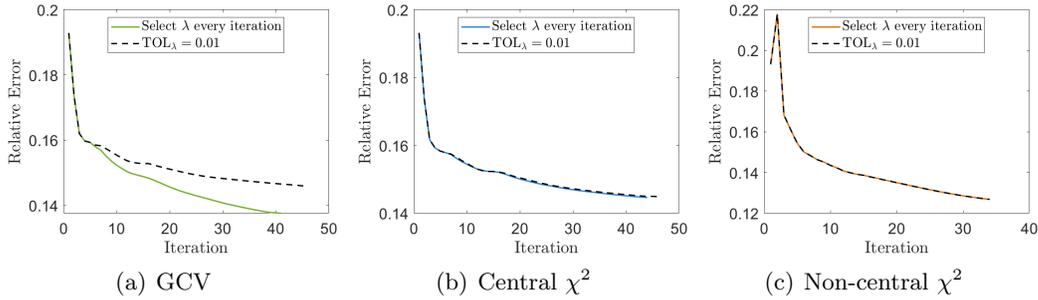(a) GCV   (b) Central χ^2 (c) Non-central χ^2

Figure 4. *RE for SB solution when $TOL_\lambda = 0.01$ compared to selecting at every iteration.*

$\mathbf{x}^{(k)}$ for $\overline{\mathbf{x}}$. Initially, we expect that $\mathbf{x}^{(k)}$ does not serve as a good estimate for $\overline{\mathbf{x}}$ to be used at step $k + 1$, because in the beginning steps the values for $\mathbf{x}^{(k)}$ are far from convergence. The bound on $F_C(\lambda)$ oscillates with λ and is largest at iteration 2 where it is 0.1. This suggests that a smaller confidence level α might be better in the early iterations when $\mathbf{x}^{(k)}$ is further from $\overline{\mathbf{x}}$ as this would increase the bound and therefore dampen the oscillations. Despite the oscillations for the early iterations, the selection of λ still converges for $\alpha = 0.999$. On the other hand, the values of λ selected by GCV and the central χ^2 dof test converge earlier. Figure 4 shows that with GCV, $\mathrm{TOL}_\lambda = 0.01$ increases the RE, but for the χ^2 dof tests, there is little change. Thus, setting a tolerance on λ is reasonable in this case.

4.1.2. Majorization-Minimization. In MM, we fix $\varepsilon = 0.0003$, which is near the suggested value in [4, 6] relative to the magnitude of $\mathbf{x}$. The ideal value of ε depends on the magnitude

(a) Relative error (b) Relative change in **x** (c) Selection of λ (d) Relative change in λ^2
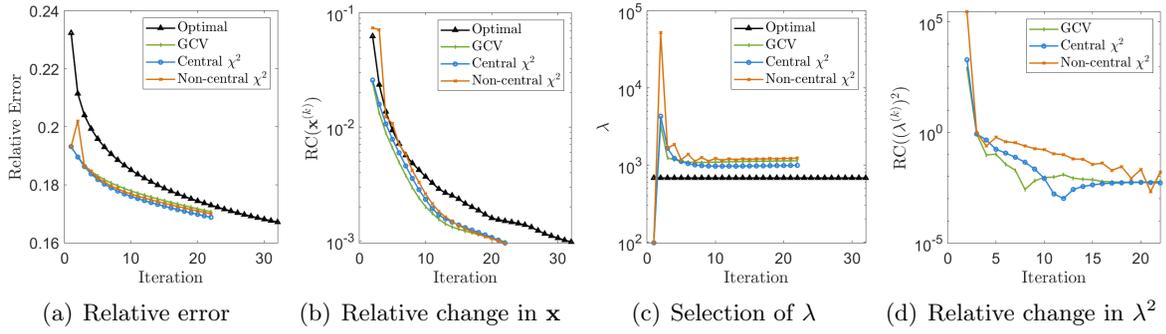
Figure 5. *Results for MM applied to Figure 1(a) where λ is fixed at the optimal $\lambda = 681.3$ or selected at each iteration with GCV or the χ^2 dof tests. Figure 5(a) plots the RE by iteration, Figure 5(b) plots the relative change in **x**, Figure 5(c) plots the λ selected, and Figure 5(d) plots the relative change in λ^2.*
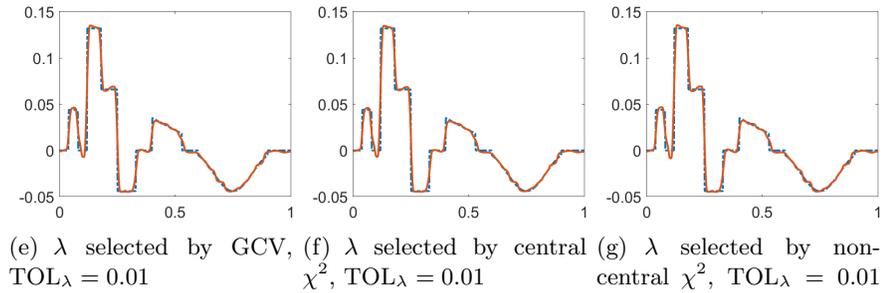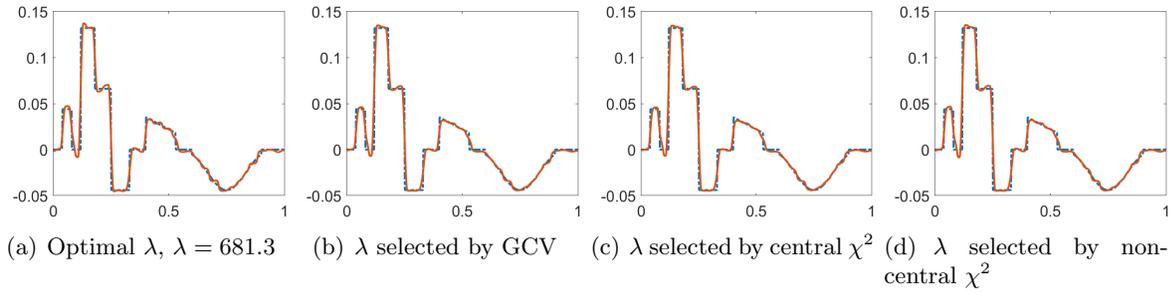

(a) Optimal λ, $\lambda = 681.3$ (b) λ selected by GCV (c) λ selected by central χ^2 (d) λ selected by non-central χ^2

(e) λ selected by GCV, $\text{TOL}_\lambda = 0.01$ (f) λ selected by central χ^2, $\text{TOL}_\lambda = 0.01$ (g) λ selected by non-central χ^2, $\text{TOL}_\lambda = 0.01$

Figure 6. *MM solutions at convergence for Figure 1(a).*

(a) GCV (b) Central χ^2 (c) Non-central χ^2
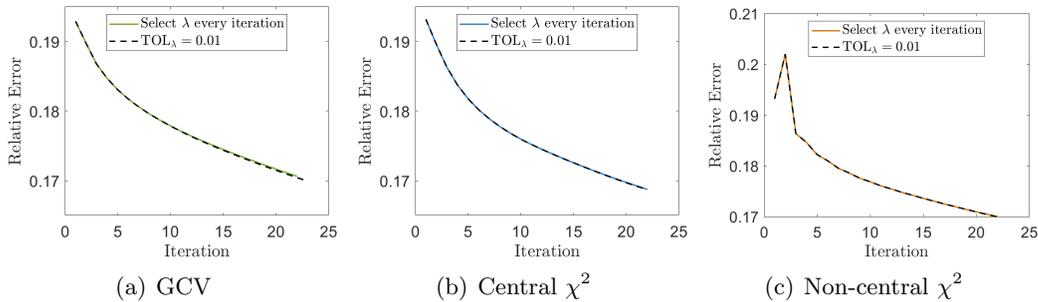
Figure 7. *RE for MM applied to Figure 1(a) with $\text{TOL}_\lambda = 0.01$ compared to selecting λ at every iteration.*

of $\mathbf{u}^{(k)} = \mathbf{L}\mathbf{x}^{(k)}$. For smaller values of ε the RE of the solution increases. In this case, the *optimal* fixed λ is $\lambda = 681.3$. The results of the selection methods are shown in Figure 5 with solutions in Figure 6. From these plots, both GCV and the χ^2 dof tests select λ well, leading to better convergence than the *optimal*. Initial values of λ found using the non-central χ^2 dof test oscillate, but still converge. The bound on $F_C(\lambda)$ changes with the oscillations, reaching a maximum of 0.068 in iteration 2. These initial steps serve to find a stabilizing value for λ that is suitable for the noise in the steps after the tolerance TOL_λ has been achieved. We set $\mathrm{TOL}_\lambda = 0.01$, after which, as seen in Figure 7, the REs of the updates decrease slowly.

4.1.3. Discussion on the one-dimensional results. The results using the SB and MM iterative methods with the regularization parameter methods are summarized in Table 1. In SB, the non-central χ^2 dof test performs best of the parameter selection methods, converging in the same number of iterations as the *optimal*. GCV and the central χ^2 dof test require more iterations to converge and have a larger RE. In MM, the three selection methods each converge in 22 iterations having approximately the same RE. They converge 10 iterations earlier than the *optimal*. In general, SB and MM are different, with SB taking longer to convergence to solutions with a smaller RE. The results suggest that the best method with respect to RE is to use SB with the non-central χ^2 dof test. Using $\mathrm{TOL}_\lambda = 0.01$ does not significantly impact the results of the selection methods.

Table 1
RE and iterations for the solutions to the 1D example in Figure 1(a)

	No TOL_λ		$\mathrm{TOL}_\lambda = 0.01$	
Method	RE	Iterations	RE	Iterations
SB, Optimal	0.126	34		
SB, GCV	0.138	41	0.146	46
SB, Central χ^2	0.145	44	0.145	45
SB, Non-central χ^2	0.127	34	0.127	34
MM, Optimal	0.167	32		
MM, GCV	0.171	22	0.170	23
MM, Central χ^2	0.169	22	0.169	22
MM, Non-central χ^2	0.170	22	0.170	22

4.2. A 2D example. For our 2D example, we use an image deblurring problem. We use the cameraman image in Figure 8(a), which is 256 by 256 pixels. The matrix $\tilde{\mathbf{A}} \in \mathbb{R}^{256^2 \times 256^2}$ now models a separable blur, defined by $\tilde{\mathbf{A}} = \frac{1}{2\pi\sigma^2}(\mathbf{C_z} \otimes \mathbf{C_z})$, where $\otimes$ defines a Kronecker product and the matrix $\mathbf{C_z}$ is a circulant matrix with first row given by (4.3) with $N = 256$, band $= 20$, and $\sigma = 2$. White Gaussian noise with SNR $= 20$ is then added to obtain $\tilde{\mathbf{b}}$. The blurred image is given in Figure 8(b) while the blurred and noisy image is given in Figure 8(c). We set $\mathbf{L} = \mathbf{D}_{2D}$, where

$$\mathbf{D}_{2D} = \begin{bmatrix} \mathbf{I} \otimes \mathbf{D}_{1D} \\ \mathbf{D}_{1D} \otimes \mathbf{I} \end{bmatrix}$$

and $\mathbf{D}_{1D} \in \mathbb{R}^{N \times N}$ is the discretization of the first derivative with periodic boundary conditions:

$$
\mathbf{D}_{1D} = \begin{bmatrix}
-1 & 1 & 0 & 0 & \cdots & 0 \\
0 & -1 & 1 & 0 & \cdots & 0 \\
\vdots & & \ddots & \ddots & & \vdots \\
0 & \cdots & 0 & -1 & 1 & 0 \\
0 & 0 & \cdots & 0 & -1 & 1 \\
1 & 0 & \cdots & 0 & 0 & -1
\end{bmatrix}.
$$

To solve this problem, we use the weighted $\mathbf{A}$ and $\mathbf{b}$ as given in (1.3). In this case, $p = 131,072$ and $n = 65,536$ so $p = 2n > n$. Instead of the GSVD, for this problem we use the discrete Fourier transform [22] for which we have the mutual decomposition

$$
\mathbf{A} = \mathcal{F}^* \mathbf{\Lambda_A} \mathcal{F}
$$

$$
\mathbf{L} = \begin{bmatrix} \mathbf{I}_N \otimes \mathbf{D}_{1D} \\ \mathbf{D}_{1D} \otimes \mathbf{I}_N \end{bmatrix} = \begin{bmatrix} \mathcal{F}^* & \mathbf{0} \\ \mathbf{0} & \mathcal{F}^* \end{bmatrix} \begin{bmatrix} \mathbf{C} \\ \mathbf{D} \end{bmatrix} \mathcal{F}.
$$

Here $\mathcal{F} \in \mathbb{C}^{n \times n}$ is the 2D discrete Fourier transform matrix, and $\mathbf{\Lambda_A}$ is a diagonal matrix with the eigenvalues of $\mathbf{A}$. The matrices $\mathbf{C} = \mathrm{diag}(c_1, \ldots, c_n)$ and $\mathbf{D} = \mathrm{diag}(d_1, \ldots, d_n)$ are diagonal and defined by $\mathbf{C} = \mathbf{I}_N \otimes \mathbf{\Lambda_L}$ and $\mathbf{D} = \mathbf{\Lambda_L} \otimes \mathbf{I}_N$, where

$$
\mathbf{\Lambda_L} = \mathrm{diag}(\lambda_1, \ldots, \lambda_N), \text{ with } \lambda_j = \exp\left(2j\pi\hat{i}/N\right) - 1, \quad j = 1, \ldots, N.
$$

The matrix $\mathbf{L}_{\mathbf{A}}^{\dagger} = \mathbf{L}^{\dagger}$ is computed as

$$
\mathbf{L}_{\mathbf{A}}^{\dagger} = \mathbf{L}^{\dagger} = \mathcal{F}^* \begin{bmatrix} \tilde{\mathbf{C}} & \tilde{\mathbf{D}} \end{bmatrix} \begin{bmatrix} \mathcal{F} & \mathbf{0} \\ \mathbf{0} & \mathcal{F} \end{bmatrix},
$$

where $\tilde{\mathbf{C}} = \mathrm{diag}\left(\tilde{c}_1, \ldots, \tilde{c}_n\right)$ and $\tilde{\mathbf{D}} = \mathrm{diag}\left(\tilde{d}_1, \ldots, \tilde{d}_n\right)$ are diagonal matrices, with

$$
\tilde{c}_i = \begin{cases} \frac{\overline{c_i}}{|c_i|^2 + |d_i|^2}, & \text{if } |c_i|^2 + |d_i|^2 \neq 0 \\ 0, & \text{if } |c_i|^2 + |d_i|^2 = 0 \end{cases}, \text{ and } \tilde{d}_i = \begin{cases} \frac{\overline{d_i}}{|c_i|^2 + |d_i|^2}, & \text{if } |c_i|^2 + |d_i|^2 \neq 0 \\ 0, & \text{if } |c_i|^2 + |d_i|^2 = 0 \end{cases}.
$$

In this case,

$$
\mathbf{L}\mathbf{L}_{\mathbf{A}}^{\dagger} = \begin{bmatrix} \mathcal{F}^* & \mathbf{0} \\ \mathbf{0} & \mathcal{F}^* \end{bmatrix} \begin{bmatrix} \mathbf{C} \\ \mathbf{D} \end{bmatrix} \begin{bmatrix} \tilde{\mathbf{C}} & \tilde{\mathbf{D}} \end{bmatrix} \begin{bmatrix} \mathcal{F} & \mathbf{0} \\ \mathbf{0} & \mathcal{F} \end{bmatrix}.
$$

This matrix is typically not the identity and has four diagonal submatrices of size $n \times n$.

As before, the selection methods are compared with the *optimal* fixed λ and a confidence level of $\alpha = 0.999$ is used in the χ^2 dof tests. This corresponds to a bound of 0.471 on $F(\lambda)$ for the central test. The bound on $F_C(\lambda)$ for the non-central test is larger, ranging from 0.471 to 0.912 in this example.
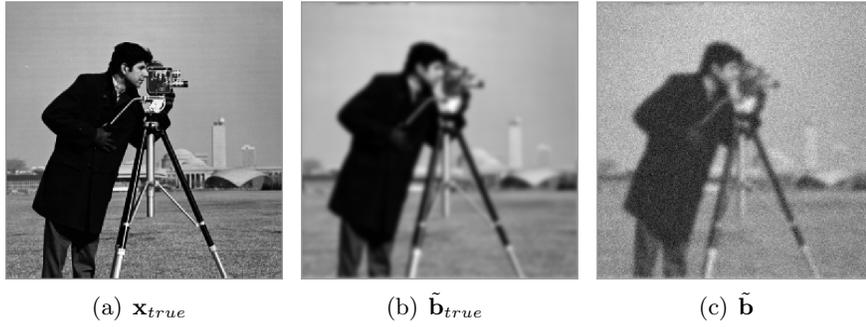
(a) $\mathbf{x}_{true}$ (b) $\tilde{\mathbf{b}}_{true}$ (c) $\tilde{\mathbf{b}}$

Figure 8. *The true image* $\mathbf{x}_{true}$, *the blurred image* $\tilde{\mathbf{b}}_{true}$, *and the blurred and noisy image* $\tilde{\mathbf{b}}$ *for the image deblurring example for image of size* 256×256.
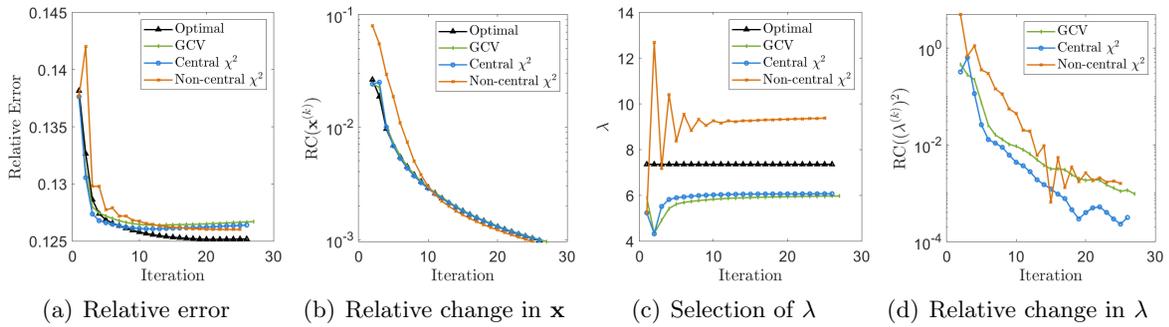

(a) Relative error   (b) Relative change in $\mathbf{x}$ (c) Selection of λ (d) Relative change in λ

Figure 9. *Results for SB applied to* Figure 8(c) *where* λ *is fixed at the optimal* $\lambda = 7.36$, *or selected at each iteration with GCV or the* χ^2 *dof tests.* Figure 9(a) *plots the RE by iteration,* Figure 9(b) *plots the relative change in* $\mathbf{x}$, Figure 9(c) *plots the* λ *selected, and* Figure 9(d) *plots the relative change in* λ^2.

4.2.1. Split Bregman. For SB, we set $\tau = 0.04$ as this leads to $RC(\mathbf{x}^{(k)})$ decreasing smoothly. The convergence results are given in Figure 9 with the solutions in Figure 10. In this case, we see that the *optimal* λ, $\lambda = 7.36$, outperforms the selection methods. The λ selected by the non-central χ^2 dof test oscillates initially, but the RE is comparable to the other methods after the third iteration. When $\text{TOL}_\lambda = 0.01$, the REs of the solutions do not change much, which is shown in Table 2.

4.2.2. Majorization-Minimization. We set $\varepsilon = 0.03$ as this is small relative to the magnitude of $\mathbf{x}$ [4, 6]. The results in Figure 11 and the reconstructions in Figure 12 show that for this ε, both GCV and the central χ^2 dof test selection methods are comparable to fixing λ at the *optimal*, $\lambda = 9.26$. The non-central χ^2 dof test does not perform as well in this case, with the values of λ oscillating widely in Figure 11(c). With $\text{TOL}_\lambda = 0.01$, the REs of the GCV and central χ^2 solutions improve, which is shown in Table 2. As a result, we do not need to select λ every iteration with MM in this case.

4.2.3. Discussion on the two-dimensional results. The results using the SB and MM iterative methods with the regularization parameter methods are summarized in Table 2. As compared to the one-dimensional results, the conclusions are the same. Namely, the best

(a) Optimal λ ($\lambda = 7.36$) (b) λ selected by GCV (c) λ selected by central χ^2 (d) λ selected by non-central χ^2

(e) λ selected by GCV, $\mathrm{TOL}_\lambda = 0.01$ (f) λ selected by central χ^2, $\mathrm{TOL}_\lambda = 0.01$ (g) λ selected by non-central χ^2, $\mathrm{TOL}_\lambda = 0.01$

Figure 10. *SB solutions at convergence for Figure 8(c).*

(a) Relative error (b) Relative change in $\mathbf{x}$ (c) Selection of λ (d) Relative change in λ
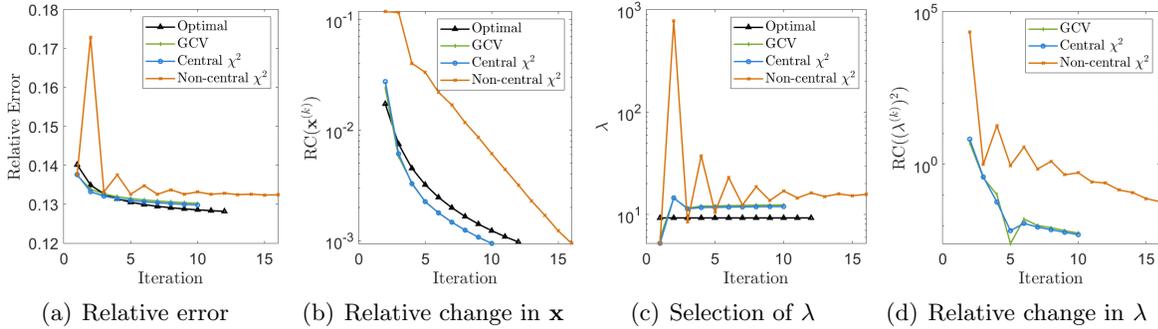
Figure 11. *Results for MM applied to Figure 8(c) where λ is fixed at the optimal $\lambda = 9.26$, or selected at each iteration with GCV or the χ^2 dof tests. Figure 11(a) plots the RE by iteration, Figure 11(b) plots the relative change in $\mathbf{x}$, Figure 11(c) plots the λ selected, and Figure 11(d) plots the relative change in λ^2.*

method is still to use SB with the non-central χ^2 dof test. Of note is that, for the MM, the non-central χ^2 dof test takes longer to converge than the *optimal*.

5. Conclusions. We have presented methods for selecting the parameters in the inner minimization problems of SB and MM by using GCV or the χ^2 dof test at each iteration, including showing a new approach to provide an estimate of the expected value of $\mathbf{x}$ each iteration, and a new theorem on the χ^2 degrees of freedom when $p > n$. For the non-central

(a) Optimal λ ($\lambda = 9.26$)   (b) λ selected by GCV   (c) λ selected by central χ^2 (d) λ selected   by   non-central χ^2

(e) λ selected by GCV, TOL$_\lambda = 0.01$ (f) λ selected by central χ^2, TOL$_\lambda = 0.01$ (g) λ selected by non-central χ^2, TOL$_\lambda = 0.01$

Figure 12. *MM solutions at convergence for Figure 8(c).*

Table 2

RE, iterations, and computation time for the solutions to the 2D example in Figure 8(c).

	No TOL$_\lambda$			TOL$_\lambda = 0.01$		
Method	RE	Iterations	Time (s)	RE	Iterations	Time (s)
SB, Optimal	0.125	26	0.4			
SB, GCV	0.127	27	26.1	0.127	27	9.4
SB, Central χ^2	0.126	26	39.3	0.127	26	11.8
SB, Non-central χ^2	0.126	25	36.6	0.126	25	19.2
MM, Optimal	0.128	12	0.2			
MM, GCV	0.130	10	9.1	0.129	11	4.7
MM, Central χ^2	0.130	10	23.0	0.129	10	11.1
MM, Non-central χ^2	0.132	16	35.7	0.132	13	38.5

χ^2 dof test, we proposed using the current solution in the iterative method as the mean of the solution. Although the parameters selected in this method vary in the early iterations, they still converge once $\mathbf{x}^{(k)}$ is closer to convergence. Numerical examples demonstrate that selecting the parameter at each iteration with these methods produces comparable results in terms of the final relative error and the number of iterations to using the *optimal* fixed

parameter. In addition, these methods do not need to be used at every iteration and can still be helpful for finding a suitable parameter in the initial iterations. They zoom in on the ideal parameter which can then be fixed after the selection method converges. This still performs well and is computationally cheaper than searching for the fixed parameters by running SB or MM to completion multiple times.

Appendix A. Derivation of the GCV function. Here, we provide the derivation of the GCV function for (1.6) and its expression in terms of the GSVD (3.3).

In GCV, λ is selected to minimize the average predictive risk when we leave out an entry of $\mathbf{b}$. Let $\mathbf{x}_\lambda^{[k]}$ be the solution when with the kth entry of $\mathbf{b}$ is missing. Then, in GCV we select λ to minimize the predictive risk for all k:

$$\min_\lambda G(\lambda) = \min_\lambda \left\{ \frac{1}{m} \sum_{k=1}^m ((\mathbf{A}\mathbf{x}_\lambda^{[k]})_k - b_k)^2 \right\}.$$

Defining the $m \times m$ matrix $\mathbf{E}_k = \text{diag}(1, 1, \ldots, 1, 0, 1, \ldots, 1)$, where the kth entry is 0, the solution $\mathbf{x}_\lambda^{[k]}$ can be written as

$$(\text{A.1}) \qquad \mathbf{x}_\lambda^{[k]} = (\mathbf{A}^\top \mathbf{E}_k^\top \mathbf{E}_k \mathbf{A} + \lambda^2 \mathbf{L}^\top \mathbf{L})^{-1} (\mathbf{A}^\top \mathbf{E}_k^\top \mathbf{E}_k \mathbf{b} + \lambda^2 \mathbf{L}^\top \mathbf{h}).$$

From the definition of $\mathbf{E}_k$, we have the following properties [10]:

$$(\text{A.2}) \qquad \mathbf{E}_k^\top \mathbf{E}_k = \mathbf{E}_k, \text{ and } \mathbf{E}_k = \mathbf{I} - \mathbf{e}_k \mathbf{e}_k^\top,$$

where $\mathbf{e}_k$ is the kth unit column vector of length m. From these properties, we obtain

$$\mathbf{A}^\top \mathbf{E}_k^\top \mathbf{E}_k \mathbf{A} + \lambda^2 \mathbf{L}^\top \mathbf{L} = (\mathbf{A}^\top \mathbf{A} + \lambda^2 \mathbf{L}^\top \mathbf{L}) - \mathbf{a}_k \mathbf{a}_k^\top = \mathbf{A_L} - \mathbf{a}_k \mathbf{a}_k^\top,$$

where $\mathbf{a}_k^\top = \mathbf{e}_k^\top \mathbf{A}$ is the kth row of $\mathbf{A}$. Then, by applying the Sherman-Morrison formula

$$(\mathbf{B} + \mathbf{u}\mathbf{v}^\top)^{-1} = \mathbf{B}^{-1} - \frac{\mathbf{B}^{-1} \mathbf{u} \mathbf{v}^\top \mathbf{B}^{-1}}{1 + \mathbf{v}^\top \mathbf{B}^{-1} \mathbf{u}}$$

to $\mathbf{B} = \mathbf{A_L}$, $\mathbf{u} = -\mathbf{a}_k$, and $\mathbf{v} = \mathbf{a}_k$, and using the first property in (A.2), we rewrite (A.1) as

$$\mathbf{x}_\lambda^{[k]} = \left(\mathbf{A_L}^{-1} + \frac{\mathbf{A_L}^{-1} \mathbf{a}_k \mathbf{a}_k^\top \mathbf{A_L}^{-1}}{1 - \mathbf{a}_k^\top \mathbf{A_L}^{-1} \mathbf{a}_k} \right) (\mathbf{A}^\top \mathbf{E}_k \mathbf{b} + \lambda^2 \mathbf{L}^\top \mathbf{h})$$

$$(\text{A.3}) \qquad = \left(\mathbf{I} + \frac{\mathbf{A_L}^{-1} \mathbf{a}_k \mathbf{a}_k^\top}{1 - \mathbf{a}_k^\top \mathbf{A_L}^{-1} \mathbf{a}_k} \right) \mathbf{A_L}^{-1} (\mathbf{A}^\top \mathbf{E}_k \mathbf{b} + \lambda^2 \mathbf{L}^\top \mathbf{h}).$$

Notice that $\mathbf{a}_k^\top \mathbf{A_L}^{-1} \mathbf{a}_k$ is the kth diagonal entry of $\tilde{\mathbf{A}}_\lambda$, which we will denote by $\tilde{a}_{kk}$. Since $(\mathbf{A}\mathbf{x}_\lambda^{[k]})_k = \mathbf{e}_k^\top \mathbf{A}\mathbf{x}_\lambda^{[k]} = \mathbf{a}_k^\top \mathbf{x}_\lambda^{[k]}$, we use (A.3) to obtain

$$
\begin{aligned}
(\mathbf{A}\mathbf{x}_\lambda^{[k]})_k &= \left(\mathbf{a}_k^\top + \frac{\mathbf{a}_k^\top \mathbf{A_L}^{-1} \mathbf{a}_k \mathbf{a}_k^\top}{1 - \mathbf{a}_k^\top \mathbf{A_L}^{-1} \mathbf{a}_k} \right) \mathbf{A_L}^{-1} (\mathbf{A}^\top \mathbf{E}_k \mathbf{b} + \lambda^2 \mathbf{L}^\top \mathbf{h}) \\
&= \left(1 + \frac{\tilde{a}_{kk}}{1 - \tilde{a}_{kk}} \right) \mathbf{a}_k^\top \mathbf{A_L}^{-1} (\mathbf{A}^\top \mathbf{E}_k \mathbf{b} + \lambda^2 \mathbf{L}^\top \mathbf{h}) \\
&= \left(\frac{1}{1 - \tilde{a}_{kk}} \right) \mathbf{e}_k^\top \mathbf{A} \mathbf{A_L}^{-1} (\mathbf{A}^\top \mathbf{E}_k \mathbf{b} + \lambda^2 \mathbf{L}^\top \mathbf{h}) \\
&= \left(\frac{1}{1 - \tilde{a}_{kk}} \right) \mathbf{e}_k^\top \mathbf{A} \mathbf{A}_\lambda^\sharp \mathbf{E}_k \mathbf{b} + \left(\frac{1}{1 - \tilde{a}_{kk}} \right) \mathbf{e}_k^\top \mathbf{A} \mathbf{L}_\lambda^\sharp \mathbf{h}.
\end{aligned}
$$

Then, by the second property in (A.2)

$$
\begin{aligned}
(\mathbf{A}\mathbf{x}_\lambda^{[k]})_k - b_k &= \left(\frac{1}{1 - \tilde{a}_{kk}} \right) \mathbf{e}_k^\top \mathbf{A} \mathbf{A}_\lambda^\sharp \mathbf{E}_k \mathbf{b} + \left(\frac{1}{1 - \tilde{a}_{kk}} \right) \mathbf{e}_k^\top \mathbf{A} \mathbf{L}_\lambda^\sharp \mathbf{h} - \mathbf{e}_k^\top \mathbf{b} \\
&= \left(\frac{1}{1 - \tilde{a}_{kk}} \right) \mathbf{e}_k^\top \mathbf{A} \mathbf{A}_\lambda^\sharp \mathbf{b} \\
&\quad - \left(\frac{\tilde{a}_{kk}}{1 - \tilde{a}_{kk}} \right) \mathbf{e}_k^\top \mathbf{b} + \left(\frac{1}{1 - \tilde{a}_{kk}} \right) \mathbf{e}_k^\top \mathbf{A} \mathbf{L}_\lambda^\sharp \mathbf{h} - \mathbf{e}_k^\top \mathbf{b} \\
&= \left(\frac{1}{1 - \tilde{a}_{kk}} \right) \mathbf{e}_k^\top \mathbf{A} \mathbf{A}_\lambda^\sharp \mathbf{b} + \left(\frac{1}{1 - \tilde{a}_{kk}} \right) \mathbf{e}_k^\top \mathbf{A} \mathbf{L}_\lambda^\sharp \mathbf{h} - \left(1 + \frac{\tilde{a}_{kk}}{1 - \tilde{a}_{kk}} \right) \mathbf{e}_k^\top \mathbf{b} \\
&= \left(\frac{1}{1 - \tilde{a}_{kk}} \right) \mathbf{e}_k^\top (\mathbf{A}\mathbf{x}_\lambda - \mathbf{b}) = \frac{(\mathbf{A}\mathbf{x}_\lambda)_k - b_k}{1 - \tilde{a}_{kk}}.
\end{aligned}
$$

Therefore, the GCV function is given by

$$
G(\lambda) = \frac{1}{m} \sum_{k=1}^m \left[\frac{(\mathbf{A}\mathbf{x}_\lambda)_k - b_k}{1 - \tilde{a}_{kk}} \right]^2.
$$

We can approximate the diagonal values of $\tilde{\mathbf{A}}_\lambda$ by the average diagonal value $\mathrm{Tr}(\tilde{\mathbf{A}}_\lambda)/m$, which produces a weighted version of the function [17]. The resulting function is then

$$
G(\lambda) = \frac{\|\mathbf{A}\mathbf{x}_\lambda - \mathbf{b}\|_2^2}{\left[\mathrm{Tr} \left(\mathbf{I} - \tilde{\mathbf{A}}_\lambda \right) \right]^2},
$$

which is the desired GCV function.

Next, we derive the formula of the GCV function (3.3) in terms of the GSVD of $\{\mathbf{A}, \mathbf{L}\}$ when $m \geq n$, given in (2.10). To do so, we first write

(A.4) $$\qquad\qquad\qquad \tilde{\mathbf{A}}_\lambda = \mathbf{A} \mathbf{A_L}^{-1} \mathbf{A}^\top = \mathbf{U} \tilde{\boldsymbol{\Upsilon}} \boldsymbol{\Phi}^{-1} \tilde{\boldsymbol{\Upsilon}}^\top \mathbf{U}^\top,$$

where $\mathbf{\Phi} = (\tilde{\mathbf{\Upsilon}}^\top \tilde{\mathbf{\Upsilon}} + \lambda^2 \tilde{\mathbf{M}}^\top \tilde{\mathbf{M}})$. The numerator then becomes

$$\begin{aligned}
\|\mathbf{A}\mathbf{x}_\lambda - \mathbf{b}\|_2^2 &= \|\mathbf{A}\mathbf{A}_\lambda^\sharp \mathbf{b} + \mathbf{A}\mathbf{L}_\lambda^\sharp \mathbf{h} - \mathbf{b}\|_2^2 \\
&= \|\mathbf{U}\tilde{\mathbf{\Upsilon}}\mathbf{\Phi}^{-1}\tilde{\mathbf{\Upsilon}}^\top \mathbf{U}^\top \mathbf{b} + \lambda^2 \mathbf{U}\tilde{\mathbf{\Upsilon}}\mathbf{\Phi}^{-1}\tilde{\mathbf{M}}^\top \mathbf{V}^\top \mathbf{h} - \mathbf{b}\|_2^2.
\end{aligned} \tag{A.5}$$

Notice that $\tilde{\mathbf{\Upsilon}}\mathbf{\Phi}^{-1}\tilde{\mathbf{\Upsilon}}^\top$ and $\lambda^2 \tilde{\mathbf{\Upsilon}}\mathbf{\Phi}^{-1}\tilde{\mathbf{M}}^\top$ are diagonal matrices, where

$$\tilde{\mathbf{\Upsilon}}\mathbf{\Phi}^{-1}\tilde{\mathbf{\Upsilon}}^\top = \begin{bmatrix} \mathbf{I}_{\tilde{n}} - \mathbf{\Psi} & \mathbf{0} & \mathbf{0} \\ \mathbf{0} & \mathbf{I}_{n-\tilde{n}} & \mathbf{0} \\ \mathbf{0} & \mathbf{0} & \mathbf{0}_{m-n} \end{bmatrix} \text{ and } \lambda^2 \tilde{\mathbf{\Upsilon}}\mathbf{\Phi}^{-1}\tilde{\mathbf{M}}^\top = \begin{bmatrix} \lambda^2 \boldsymbol{\zeta} & \mathbf{0} \\ \mathbf{0} & \mathbf{0}_{(m-\tilde{n})\times(p-\tilde{n})} \end{bmatrix} \tag{A.6}$$

with $\mathbf{\Psi}, \boldsymbol{\zeta} \in \mathbb{R}^{\tilde{n}\times\tilde{n}}$ defined in (3.7). Factoring out the orthogonal matrix $\mathbf{U}$ from (A.5), we obtain

$$\begin{aligned}
&\|\mathbf{U}\tilde{\mathbf{\Upsilon}}\mathbf{\Phi}^{-1}\tilde{\mathbf{\Upsilon}}^\top \mathbf{U}^\top \mathbf{b} + \lambda^2 \mathbf{U}\tilde{\mathbf{\Upsilon}}\mathbf{\Phi}^{-1}\tilde{\mathbf{M}}^\top \mathbf{V}^\top \mathbf{h} - \mathbf{b}\|_2^2 \\
&= \|(\tilde{\mathbf{\Upsilon}}\mathbf{\Phi}^{-1}\tilde{\mathbf{\Upsilon}}^\top - \mathbf{I}_m)\mathbf{U}^\top \mathbf{b} + \lambda^2 \tilde{\mathbf{\Upsilon}}\mathbf{\Phi}^{-1}\tilde{\mathbf{M}}^\top \mathbf{V}^\top \mathbf{h}\|_2^2 \\
&= \left\| \sum_{i=1}^{\tilde{n}} \frac{\lambda^2 \gamma_i (\mathbf{v}_i^\top \mathbf{h})}{\gamma_i^2 + \lambda^2} - \sum_{i=1}^{\tilde{n}} \frac{\lambda^2 (\mathbf{u}_i^\top \mathbf{b})}{\gamma_i^2 + \lambda^2} - \sum_{i=n+1}^{m} \mathbf{u}_i^\top \mathbf{b} \right\|_2^2,
\end{aligned}$$

where we ignore any sum where the lower limit is greater than the upper limit. In the denominator, we can use (A.4) and (A.6) to obtain the desired result,

$$\begin{aligned}
\left[\mathrm{Tr}\left(\mathbf{I} - \tilde{\mathbf{A}}_\lambda \right) \right]^2 &= \left[\mathrm{Tr}\left(\mathbf{I} - \mathbf{U}\tilde{\mathbf{\Upsilon}}\mathbf{\Phi}^{-1}\tilde{\mathbf{\Upsilon}}^\top \mathbf{U}^\top \right) \right]^2 \\
&= \left[\mathrm{Tr}\left(\mathbf{I} - \tilde{\mathbf{\Upsilon}}\mathbf{\Phi}^{-1}\tilde{\mathbf{\Upsilon}}^\top \right) \right]^2 = \left[\sum_{i=1}^{\tilde{n}} \frac{\lambda^2}{\gamma_i^2 + \lambda^2} + \max(m-n, 0) \right]^2.
\end{aligned}$$

REFERENCES

[1] M. ALOTAIBI, A. BUCCINI, AND L. REICHEL, *Restoration of blurred images corrupted by impulse noise via median filters and ℓ_p-ℓ_q minimization*, in 2021 21st International Conference on Computational Science and Its Applications (ICCSA), IEEE, 2021, pp. 112–122.

[2] R. C. ASTER, B. BORCHERS, AND C. H. THURBER, *Parameter Estimation and Inverse Problems*, Elsevier, Amsterdam, 2018.

[3] T. BONESKY, *Morozov's discrepancy principle and Tikhonov-type functionals*, Inverse Problems, 25 (2008), p. 015015.

[4] A. BUCCINI, G. HUANG, L. REICHEL, AND F. YIN, *On the choice of regularization matrix for an ℓ^2-ℓ^q minimization method for image restoration*, Appl. Numer. Math., 164 (2021), pp. 211–221.

[5] A. BUCCINI, M. PRAGLIOLA, L. REICHEL, AND F. SGALLARI, *A comparison of parameter choice rules for ℓ_p-ℓ_q minimization*, Annali Dell'Universita'di Ferrara, 68 (2022), pp. 441–463.

[6] A. BUCCINI AND L. REICHEL, *An ℓ^2-ℓ^q regularization method for large discrete ill-posed problems*, J. Sci. Comput., 78 (2019), pp. 1526–1549.

[7] A. BUCCINI AND L. REICHEL, *An ℓ_p-ℓ_q minimization method with cross-validation for the restoration of impulse noise contaminated images*, J. Comput. Appl. Math., 375 (2020), p. 112824.

[8] M. J. BYRNE AND R. A. RENAUT, *Learning spectral windowing parameters for regularization using unbiased predictive risk and generalized cross validation techniques for multiple data sets*, Inverse Probl. Imaging, 17 (2023).

[9] J.-F. Cai, S. Osher, and Z. Shen, *Linearized Bregman iterations for frame-based image deblurring*, SIAM J. Imaging Sci., 2 (2009), pp. 226–252.

[10] J. Chung, G. Easley, and D. P. O'Leary, *Windowed spectral regularization of inverse problems*, SIAM J. Sci. Comput., 33 (2011), pp. 3175–3200.

[11] J. Chung and M. I. Español, *Learning regularization parameters for general-form Tikhonov*, Inverse Problems, 33 (2017), p. 074004.

[12] J. Chung, M. I. Español, and T. Nguyen, *Optimal regularization parameters for general-form Tikhonov regularization*, arXiv preprint arXiv:1407.1911, (2014).

[13] L. Eldén, *A weighted pseudoinverse, generalized singular values, and constrained least squares problems*, BIT Numerical Mathematics, 22 (1982), pp. 487–502.

[14] E. Esser, *Applications of Lagrangian-based alternating direction methods and connections to split Bregman*, CAM report, 9 (2009), p. 31.

[15] H. Fang and H. Zhang, *Wavelet-based double-difference seismic tomography with sparsity regularization*, Geophysical Journal International, 199 (2014), pp. 944–955.

[16] T. Goldstein and S. Osher, *The split Bregman method for ℓ_1-regularized problems*, SIAM J. Imaging Sci., 2 (2009), pp. 323–343.

[17] G. H. Golub, M. Heath, and G. Wahba, *Generalized cross-validation as a method for choosing a good ridge parameter*, Technometrics, 21 (1979), pp. 215–223.

[18] G. H. Golub and C. F. Van Loan, *Matrix Computations*, Johns Hopkins University Press, Baltimore, MD, 1983.

[19] P. C. Hansen, *Analysis of discrete ill-posed problems by means of the L-curve*, SIAM Rev., 34 (1992), pp. 561–580.

[20] P. C. Hansen, *Rank-deficient and Discrete Ill-posed Problems: Numerical Aspects of Linear Inversion*, SIAM, Philadelphia, 1998.

[21] P. C. Hansen, *Discrete Inverse Problems: Insight and Algorithms*, SIAM, Philadelphia, 2010.

[22] P. C. Hansen, J. G. Nagy, and D. P. O'Leary, *Deblurring Images: Matrices, Spectra, and Filtering*, SIAM, Philadelphia, 2006.

[23] R. Hou, Y. Xia, Y. Bao, and X. Zhou, *Selection of regularization parameter for l1-regularized damage detection*, Journal of Sound and Vibration, 423 (2018), pp. 141–160.

[24] P. Howland and H. Park, *Generalizing discriminant analysis using the generalized singular value decomposition*, IEEE Transactions on Pattern Analysis and Machine Intelligence, 26 (2004), pp. 995–1006.

[25] G. Huang, A. Lanza, S. Morigi, L. Reichel, and F. Sgallari, *Majorization–minimization generalized Krylov subspace methods for $\ell_p - \ell_q$ optimization applied to image restoration*, BIT Numerical Mathematics, 57 (2017), pp. 351–378.

[26] D. R. Hunter and K. Lange, *A tutorial on MM algorithms*, Amer. Statist., 58 (2004), pp. 30–37.

[27] B. Jin, Y. Zhao, and J. Zou, *Iterative parameter choice by discrepancy principle*, IMA J. Numer. Anal., 32 (2012), pp. 1714–1732.

[28] C. L. Mallows, *Some comments on C_p*, Technometrics, 42 (2000), pp. 87–94.

[29] J. Mead, *χ^2 test for total variation regularization parameter selection*, Inverse Probl. Imaging, 14 (2020).

[30] J. L. Mead, *Parameter estimation: A new approach to weighting a priori information*, J. Inv. Ill-posed Problems, 16 (2008), pp. 175–194.

[31] J. L. Mead and R. A. Renaut, *A Newton root-finding algorithm for estimating the regularization parameter for solving ill-conditioned least squares problems*, Inverse Problems, 25 (2008), p. 025002.

[32] V. A. Morozov, *On the solution of functional equations by the method of regularization*, in Doklady Akademii Nauk, vol. 167, Russian Academy of Sciences, 1966, pp. 510–512.

[33] M. Pasha, *Krylov Subspace Type Methods for the Computation of Non-negative or Sparse Solutions of Ill-posed Problems*, PhD thesis, Kent State University, Kent, OH, 2020.

[34] R. A. Renaut, I. Hnětynková, and J. Mead, *Regularization parameter estimation for large-scale Tikhonov regularization using a priori information*, Comput. Statist. Data Anal., 54 (2010), pp. 3430–3445.

[35] L. I. Rudin, S. Osher, and E. Fatemi, *Nonlinear total variation based noise removal algorithms*, Phys. D, 60 (1992), pp. 259–268.

[36] R. J. Tibshirani and J. Taylor, *Degrees of freedom in lasso problems*, Ann. Statist., (2012).

[37] A. N. Tikhonov and V. Y. Arsenin, *Solution of incorrectly formulated problems and the regularization method*, Soviet Math. Dokl., 5 (1963), pp. 1035–1038.

[38] S. Vatankhah, R. A. Renaut, and V. E. Ardestani, *Regularization parameter estimation for underdetermined problems by the χ^2 principle with application to 2D focusing gravity inversion*, Inverse Problems, 30 (2014), p. 085002.

[39] G. Wang, J. Xu, Z. Pan, and Z. Diao, *Ultrasound image denoising using backward diffusion and framelet regularization*, Biomedical Signal Processing and Control, 13 (2014), pp. 212–217.

[40] H. Yao, P. Gerstoft, P. M. Shearer, and C. Mecklenbräuker, *Compressive sensing of the Tohoku-Oki Mw 9.0 earthquake: Frequency-dependent rupture modes*, Geophysical Research Letters, 38 (2011).